Journal of Translational Medicine

RESEARCH

Open Access

Rasal2 inhibits autophagic-exosomes secretion via regulating Rab27a in triple-negative breast cancer progression

Xuan Wang[1*†], Guocui Qi[1†], Kunning Yang[2], Linlin Ma[1], Yuansai Kang[1], Xiaojing Tang[1] and YanTao Han[1*]

Abstract

Background Triple-negative breast cancer (TNBC) is a subtype with the worst prognosis and there is still a lack of effective treatment. Exosomes (Exos) secreted by cancer cells to tumor microenvironment play an important role in cancer progression. We have demonstrated that the function of Rasal2 in the modulation of breast cancer progression is exos-mediated, but the relationship between Rasal2 and exosome secretion remains elusive.

Methods Rasal2 knock-out (KO) MDA-MB-231 cells were conducted by crispr-cas9 technique and Rab27a knock-down (KD) in Rasal2 KO MDA-MB-231 cells (KO + KD) were further established by siRNA-mate plus transfection Reagent. Control (CT)/KO MDA-MB-231 cells stably overexpressing GFP-LC3 were generated by using GFP-LC3 plamisd. Transmission electron microscope (TEM), nanoparticle tracking analysis (NTA) and western blot analysis (WB) were used to identify exos derived from TNBC. Confocal microscopy was used to observe the autophagic flux and the colocalization of autophagosomes and multivesicular bodies (MVBs). Co-immunoprecipitation analysis was performed to determine the interaction between Rasal2 and Rab27a. Immunohistochemical analysis were used to detect the expression levels of autophagy-related proteins in tumor tissues of xenograft mice inoculated with CT/KO/KO + KD MDA-MB-231 cells.

Results In this paper, we found that Rasal2 KO disrupts autophagic flux and induces secretory autophagy to promote autophagic-exos secretion in TNBC. Moreover, Rasal2 inhibits the activity of Rab27a which regulates vesicles transport and fusion, and Rab27a mediates Rasal2 KO-induced autophagic-exos secretion. Additionally, Rab27a KD inhibits Rasal2 KO-induced secretory autophagy, thereby promoting TNBC progression both in vivo and in vitro.

Conclusions Collectively, these findings delineated the role of Rab27a in TNBC progression modulated by Rasal2 through autophagy-exos pathway and suggested that it is of great significance for the early diagnosis, targeted therapy and prognosis judgement of TNBC from the perspective of tumor microenvironment.

Keywords Rasal2, Rab27a, Secretory autophagy, Autophagic-exos, TNBC progression

†Xuan Wang and Guocui Qi contributed equally to this work.

*Correspondence:
Xuan Wang
wx105yxz@163.com
YanTao Han
hanyt@qdu.edu.cn

Full list of author information is available at the end of the article

Graphical Abstract

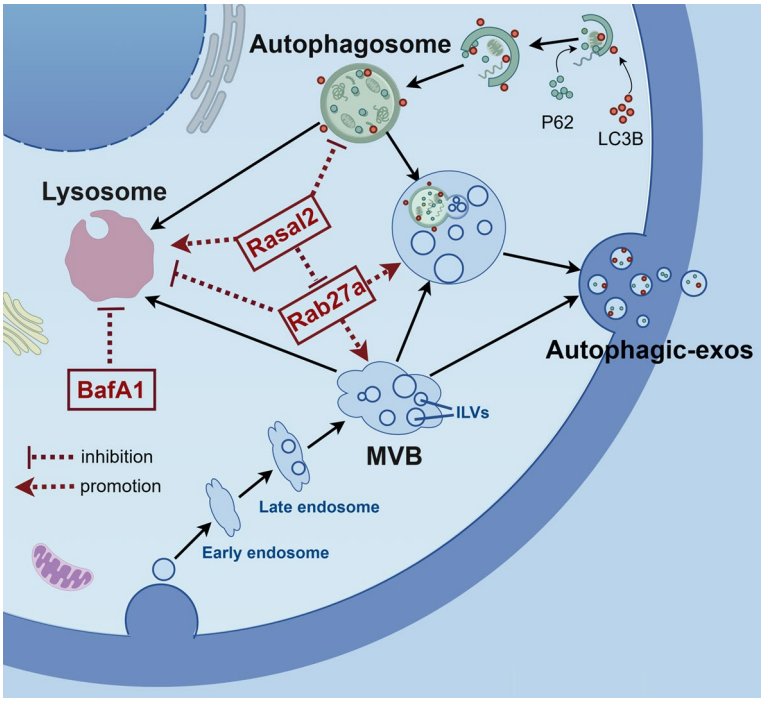

Introduction

Breast cancer is one of the most common malignancies in women worldwide and remains the number one killer of cancer death among women [1, 2]. TNBC, characterized with the negative expression of estrogen receptor (ER), progesterone receptor (PR) and human epidermal growth factor receptor 2 (HER2), accounts for about 15–20% of all breast cancers and is the most challenging subtype of breast cancer with higher heterogeneity and stronger aggressiveness than other breast cancer subtypes [3, 4]. Therefore, it is of great significance to gain insight into the molecular mechanisms of TNBC progression and explore the new prevention and effective treatment [5, 6].

Rasal2 (Ras Protein Activator Like 2), an important member of the RASGAPs proteins, has been shown to have tumor-type-dependent opposite regulatory effects on tumor progression, even has different functions for different subtypes of the same tumor, such as breast cancer [7–9]. Rasal2 has been reported to be a tumor suppressor in typical ER-positive (ER+) luminal type breast cancer and be absent in 50% of breast tumors [10]. In addition, Rasal2 KO promoted the growth and metastasis of luminal mammary tumors in mice models. However, there are accumulating evidence suggesting an oncogenic role of Rasal2 in TNBC, as opposed to its effect in ER + luminal breast cancer [11, 12]. Further studies also showed that Rasal2 expression was up-regulated in TNBC and anti-invasive miR-136 inhibited epithelial-mesenchymal transformation (EMT) by targeting Rasal2 [13]. Moreover, our previous study has confirmed that exosomes (exos) mediates the regulatory effect of Rasal2 on breast cancer progression [14, 15]. However, the relationship between Rasal2 and exos secretion from breast cancer cells is still unknown, and relevant research need to be further conducted.

Exos are small extracellular vesicles (EVs) with a diameter of approximately 30–150 nm produced by cells through endocytosis, then gradually evolved into multivesicular bodies (MVBs) with intraluminal vesicles (ILVs), and eventually secreted as exos after the fusion of MVBs with the plasma membrane [16–18]. Exos naturally exist in almost all body fluids such as blood or cell culture medium [19, 20] and contain a variety of biological functional molecules such as proteins, lipids and nucleic acids [21, 22], carrying plenty of substances that can reflect the characteristics of parental cells. Therefore, exos may become a potential modality of tumor diagnosis and treatment. In our previous study, we found large amounts of autophagy-related proteins were accumulated in exos derived from Rasal2-KO MCF-7 breast cancer cells (ER+) [15]. Nevertheless, it is currently unknown whether that is the case in TNBC cells.

Autophagy is a major metabolic and homeostatic pathway that has been described as a manner for cells to maintain cell survival by using the acidic environment of the lysosomes to degrade damaged, denatured or

senescent proteins and organelles in stressful situations such as insufficient nutrition [23, 24]. More and more evidence shows that process of autophagy formation and vesicle transport have multiple intersection, autophagosomes formed during autophagy are not only transported to lysosomes for degradation, but also released as exos (autophagic-exos) by fusion with MVBs when lysosomal dysfunction or autophagosome degradation is blocked [25, 26]. Accumulating studies focused on not only the intrinsic functions of autophagy in tumour cells, but also the important roles of autophagy in the tumour microenvironment [27–29]. Therefore, we speculated that the accumulation of autophagy-related proteins in breast cancer cell-derived exos mentioned above might be caused by its regulation of autophagy.

The Rabs, the largest family of mammalian membrane transporters with GTPases activity, are involved in various steps of membrane transport, including vesicles transport and docking, the fusion of vesicles with receptor membranes, and the control of multiple cellular functions such as cell proliferation, invasion, signal transduction and exosomal secretion [30, 31]. Rab27a, responsible for the docking and fusion of MVBs with the plasma membrane, is the main regulator of exos secretion [32, 33]. However, Rab proteins also participate in autophagy formation in addition to playing a molecular "switch" role in membrane transport [34, 35]. In view of the cross role of Rab27a in the process of autophagy and exos formation, we hypothesized that Rab27a might mediate Rasal2-regulated exos secretion.

In this paper, we explored the molecular mechanism of Rasal2 in regulating autophagy and exos secretion in vivo and in vitro experiments and clarified the role of Rab27a in the effect of TNBC progression modulated by Rasal2 through autophagy-exosomal pathway, which is expected to further illustrate the regulation mechanism of Rasal2 in TNBC progression from the perspective of tumor microenvironment and is of great significance for the early diagnosis, targeted therapy and prognosis judgment of TNBC.

Materials and methods

Cell lines and reagents

Human TNBC cell lines (BT-549, HCC1937 and MDA-MB-231) and non-tumoral human breast epithelial cell line (MCF10A) were obtained from American Type Culture Collection (ATCC), HEK-293T cell line was obtained from GE lifesciences (Buckinghamshire, UK). MCF10A cell lines were cultured in MCF10A cell special medium and other cell lines were separately cultured in RPMI 1640 medium and Dulbecco's Modified Eagle's Medium supplemented with 10% fetal bovine serum (FBS), and maintained in an incubator containing 5% CO_2 at 37 ℃. The following reagents were commercially obtained: Bafilomycin A1 (BafA1) was from TargetMol (Shanghai, China); GW4869 was from Sigma-Aldrich (MO, USA); Rab27a siRNA and siRNA-mate plus transfection reagent were from GenePharma (Suzhou, China); The eukaryotic expression vector pcDNA3.1 (+) encoding Rab27a was purchased from GENCEFE Biotech (Wuxi, China); EGFP-LC3B and PBABE-puro mcherry-EGFP-LC3B plasmids were from Wuhan Miaoling Biotechnology (Wuhan, China); Lipofectamine 2000 Reagent was from Thermo Fisher (MA, USA); Lyso-Tracker Green was from Beyotime Biotechnology (Shanghai, China). Antibodies against P62, LC3AB, GAPDH and Goat Anti-Rabbit IgG (H + L) (peroxidase/HRP conjugated) were from Elabscience (Houston, USA); Antibodies against CD9, TSG101, ALIX and CD63 were from Abcam (MA, USA); the antibody against Rasal2 was from proteintech (Chicago, USA); the antibodies against calnexin and β-actin were from Cell Signaling Technology (MA, USA); the antibody against HSP70 was from Zenbio (Chengdu, China); the antibody against Rab27a was from Fine Test (Wuhan, China); the antibody against Myc was from Santa Cruz Biotechnology (TX, USA); the antibody against Flag was from Sigma (MO, USA); Animal experiment was authorized by the Animal Ethical Committee of Qingdao University.

Establishment of Rasal2 knockout (KO) cell lines and Rab27a knockdown (KD) cell lines

Rasal2 KO MDA-MB-231 cell lines were established by CRISPR/Cas9 gene-editing technique. gRNA sequences of Rasal2: gRNA-A1: 5′-CATGCTGGGAGGTTTCTT CAAGG-3′; gRNA-A2: 5′-GACCACCTCAGATCTATC AGTGG-3′. The synthesized gRNA (RNP complex) was transfected into MDA-MB-231 cells by electrotransfer technique using Neon™ transfection system device and stable KO cell lines were generated by the selection of monoclonal population of cells.

Rasal2 KO/Rab27a KD (KO + KD) MDA-MB-231 cell lines were established by siRNA-mate plus transfection Reagent. siRNA sequence of Rab27a: 5′-GGAGAGGUU UCGUAGCUUATT-3′. Rab27a siRNA was transfected into Rasal2 KO MDA-MB-231 cell lines by transfection reagent to generate transient (KO + KD) MDA-MB-231 cells.

EVs separation and purification

EVs were separated and purified from MDA-MB-231 cell culture supernatant by differential ultracentrifugation (UC) according to the protocol from Théry C et al. [36]. In brief, cells were cultured in DMEM supplemented with 10% exos-depleted FBS for 24 h, then the supernatant was collected and centrifuged at 300×g for 10 min to remove cells, after which the supernatant was subjected to sequential centrifugation at 2,000×g for 10 min

and 10,000×g for 20 min to remove dead cells and cell debris, respectively. The resulting supernatants were filtered using a 0.2 μm filter, followed by ultracentrifugation at 100,000×g for 70 min. Again, the pellets were resuspended in PBS and ultracentrifuged at 100,000×g for 70 min. All centrifugations were carried out at 4 °C.

Nanoparticle tracking analysis (NTA)

The size distribution of the purified particles was detected using NanoSight NS300 (Malvern Panalytical Ltd., Malvern, UK) equipped with an NanoSight Software (NTA version 3.3.301). In brief, the purified particles were diluted in PBS to adjust their concentration (30–100 particles/frame) within the linear range of the instrument as recommended by the manufacturer before NTA analysis, then the diluted sample was taken up with a syringe and introduced into the chamber. Then the diameter (nM) and the concentration (particles/mL) of the particles were detected and analyzed.

Transmission electron microscopy (TEM)

TEM was carried out to observe the morphology and the size of the purified samples as previously described [36]. In brief, the samples were adsorbed onto the formvar coated grids and then fixed with 4% glutaraldehyde, after which the samples were stained with 2% uranyl acetate (UA). The grids were finally analyzed and the images were captured by a JEOL JEM-1400 transmission electron microscopy (JEOL, Tokyo, Japan) equipped with a digital photomicrograph ORIUSTM SC1000 CCD camera (GATAN Inc., Pleasanton, California).

Colony formation assay

Cell proliferation capacity was detected by a clonogenic assay as described. Briefly, MDA-MB-231 cells (Control (CT), KO, KO + KD) were trypsinized and seeded into a six-well plate at a density of 800 cells/well in triplicate. After incubation at 37℃ for 14 days, the cells were fixed and stained with 0.1% crystal violet to visualize colonies. Colonies were photographed and colony number was counted manually.

Wound healing assay

Cell migration was evaluated by scratch wound assay as described. Briefly, MDA-MB-231 cells (CT, KO, KO + KD) were inoculated in 6-well plates and cultured into monolayers, then a scratch wound of the monolayers was generated by using a sterile 200 μL pipette tip and the floating cells were removed by washing with PBS. The scratches were photographed under an inverted microscope (Leica microsystems, Wetzlar, Germany) at different times (0, 24 h) after scratching. The scratch gap distance was quantitatively measured by Image J software and the scratch healing rate was calculated.

Transwell assay

Transwell plates coated with or without Matrigel reagent (BD bioscience, SanJose, CA) were used to analyze the ability of cell invasion and migration, separately. Briefly, MDA-MB-231 cells (CT, KO, KO + KD) suspended in serum-free medium were added to the upper compartments and culture medium plus 10% FBS was added to the lower compartments. After cultivation for 24 h, the upper compartments was cleaned with a cotton swab to remove cells, the lower compartments was fixed with 4% paraformaldehyde and stained with 0.5% crystal violet (Sigma). Then the migrated cells were imaged and manually counted under an inverted microscope (Zeiss, Germany). The procedures for the cell invasion were the same as for the cell migration except that the upper compartment was precoated with 100 μl of Matrigel. Transwell assay was conducted three times with three biological repetitions each time.

Western blot analysis

Proteins expression was detected by western blotting. Total proteins were prepared with RIPA buffer (Elabscience) and the concentrations of protein samples were determined using BCA reagent kit (Elabscience). The equal proteins were fractionated by SDS/PAGE gels and transferred to 0.45 μm PVDF membrane (Solarbio). After sealing with 5% skimmed milk, the membrane was incubated with the indicated primary antibodies at 4 °C overnight and then incubated with horseradish-peroxidase-conjugated secondary antibody for 1 h at room temperature. Afterwards, the protein bands were visualized by enhanced chemiluminescence and quantified by the Image J software (National Institutes of Health, Bethesda, MD, USA).

Autophagic flux analysis

Autophagic flux was evaluated by PBABE-puro mcherry-EGFP-LC3B plasmid (Miaoling, Wuhan, China). The plasmid was transfected into MDA-MB-231 cells (CT, KO, KO + KD) by Lipofectamine 2000 (Thermo Fisher) according to the manufacturer's protocols. After transfection for 18 h, the cells were treated with BafA1 for 6 h and the images acquisition was performed by using STELLARIS 5 confocal microscopy (Leica, Germany). Then autolysosomes (red puncta) and autophagosomes (yellow puncta) per cell were quantified from at least 10 cells in three independent experiments and the proportions of autophagosomes and autolysosomes were calculated respectively to indicate autophagic flux.

Lyso-tracker assay

Lysosomal acidity was detected by acidotropic fluorescent probe Lyso-Tracker Green according to the manufacturer's instructions (Beyotime, Shanghai, China).

Briefly, MDA-MB-231 cells (CT, KO, KO + KD) were seeded and incubated with Lyso-Tracker Green solution (50 nM) at 37℃ for 60 min. The nucleus was dyed with DAPI after staining. Then the cells were observed and the images were acquired by using STELLARIS 5 confocal microscopy (Leica, Germany).

Immunofluorescence analysis

Immunofluorescence analysis was conducted to observe the colocalization of autophagosomes and MVBs as previously described [37]. Briefly, MDA-MB-231 cells (CT, KO, KO + KD) were seeded and transfected with EGFP-LC3 plasmid for 24 h. The medium was removed and the cells were washed with PBS. Subsequently, the cells were fixed with 4% paraformaldehyde for 15 min, permeabilized with 0.1% Trition-X at room temperature for 10 min, blocked with 10% BSA for 1 h, and then incubated with anti-CD63 antibody overnight, followed by incubation with goat anti-Mouse IgG (H + L) for 1 h. The cells were observed under a STELLARIS 5 confocal microscopy (Leica, Germany) and the images were obtained and analyzed using the Image J software.

Co-immunoprecipitation analysis (Co-IP)

Co-IP analysis was conducted as described by the protocol of a standard method [38]. Briefly, the cells were seeded and transfected by Lipofectamine 2000. The cell lysates were extracted with a RIPA buffer and the immunoprecipitates were then formed by binding the target protein with the indicated antibody and incubating with anti-Flag (M2) antibody-conjugated beads or GTP beads overnight at 4 ℃. Finally, the immunoprecipitates were washed and electrophoresed on SDS-PAGE gels, transferred to a PVDF membrane, probed with the antibodies, and visualized with enhanced chemiluminescence.

Immunohistochemical analysis (IHC)

IHC was used to detect the expression of proliferation-associated and autophagy-related proteins in tumor tissues. Briefly, fresh tumor tissues fixed with 4% paraformaldehyde for 24 h was embedded in paraffin and cut into 5 mm paraffin sections. Immunohistochemical staining was performed with the rapid immunohistochemical kit (Elabscience, China). Antibodies used in IHC were P62 (1:100), LC3 (1:100) and Ki67 (1:400). After reacting with biotinylated secondary antibody, DAB staining was performed. Then the sections were observed and imaged under the Panoramic Tissue Cell Scanning Analyzer (Pannoramic MIDI, Hungary).

Xenograft model assay

A total of 18 BALB/c female nude mice were purchased from Vital River Laboratory Animal Technology (Beijing, China). All nude mice were randomly divided into three groups ($n = 6$) and subcutaneously injected with MDA-MB-231 cells (CT, KO, KO + KD), individually. The dimension (width and length) of tumors and the weight of mice in each group were measured every 6 d and the tumor volume was calculated as (width × width × length)/2. At 42 d, blood was collected by eyeball enucleation before the mice were sacrificed. Then the exos were extracted from the serum separated from blood and the expression of autophagic and exosomal marker proteins in exos was detected by western blot analysis. Additionally, immunohistochemistry (IHC) assay was performed to determin the expression levels of Ki67, P62 and LC3 in tumor tissues after the tumors were photographed and weighed.

Statistical analysis

Data analysis was performed using GraphPad Prism software (La Jolla, CA, USA). The results were presented as means ± standard deviation (SD). Statistical significance between groups was determined by One-way ANOVA or Student's t-test. A p-value less than 0.05 was considered to be a significant difference.

Results

Isolation and identification of exos

To detect the secretion of exos from TNBC cells, differential ultracentrifugation was used to isolate and purify EVs from the supernatants of MDA-MB-231 cells (Fig. 1a). Then the EVs were characterized and identified by NTA and TEM. As shown by NTA, the overall particle size distribution ranged from 50 to 200 nm (Fig. 1b), and the average ζ-potential of EVs was − 9.92 mv, the same as the surface potential of the cell membrane (Fig. 1c). Consistent with NTA, the image of TEM displayed that the morphology of EVs is round or oval in shape with the diameter of approximately 30–100 nm (Fig. 1d). Additionally, WB analysis of EVs detected the positive expression of CD9, CD63, HSP70, ALIX and TSG101, served as typical biomarkers of exos, but no expression of the negative marker protein calnexin (Fig. 1e). All the results above confirmed that the isolated EVs were actually exos.

Loss of Rasal2 promotes autophagic-exos secretion in TNBC

To explore the effect of Rasal2 on exos secretion from TNBC cells, Rasal2 KO MDA-MB-231 cells were constructed using CRISPR/Cas9 technique and verified by sequencing and WB analysis (Fig. 2a-b). Then the result of NTA showed Rasal2 KO significantly increased exos secretion (Fig. 2c). In addition, we found that Rasal2 KO cells-derived exos exhibited the higher expression levels of exos marker proteins (CD63 and HSP70) and autophagy marker proteins (LC3 and P62) than those expressed in CT group by using WB analysis and further affirmed

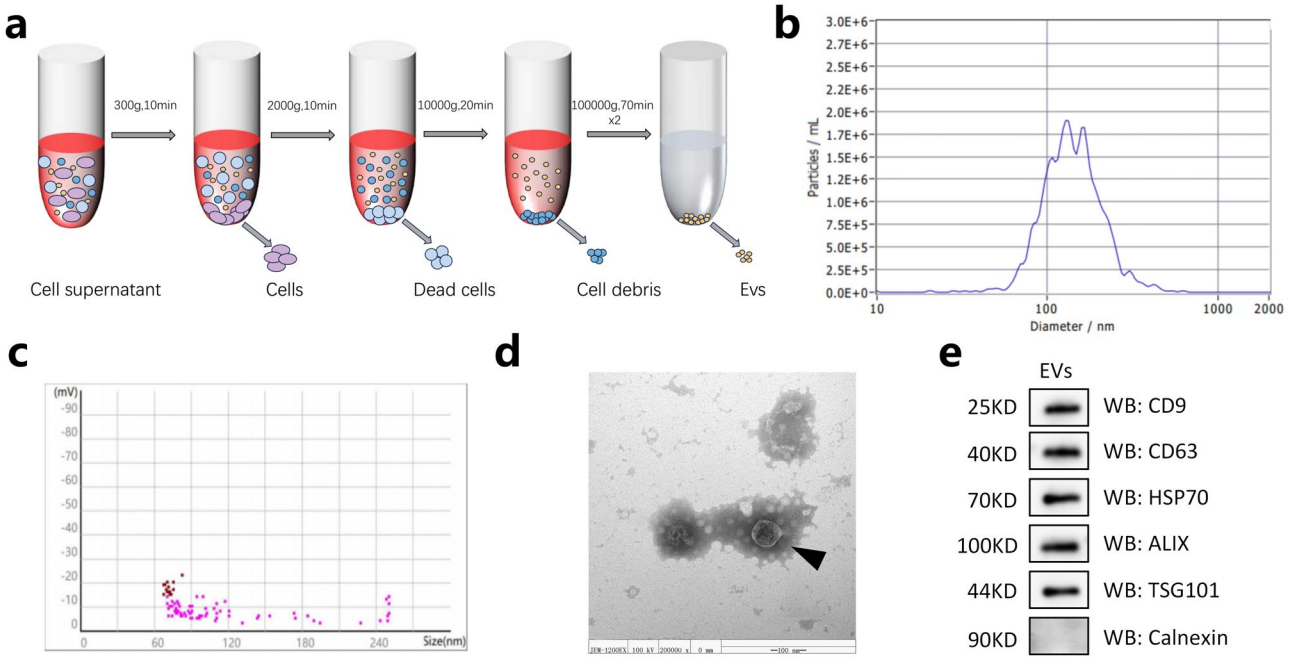

Fig. 1 Isolation and identification of exos. **a**, Isolation and purification of EVs from the conditioned media by ultracentrifugation. **b**, Size distribution of EVs analyzed by NTA. **c**, The ζ-potential of EVs. **d**, The morphology of EVs characterized by TEM, Scale bar = 100 nm. **e**, Proteins expression of exosomal positive and negative biomarkers detected by western blot analysis

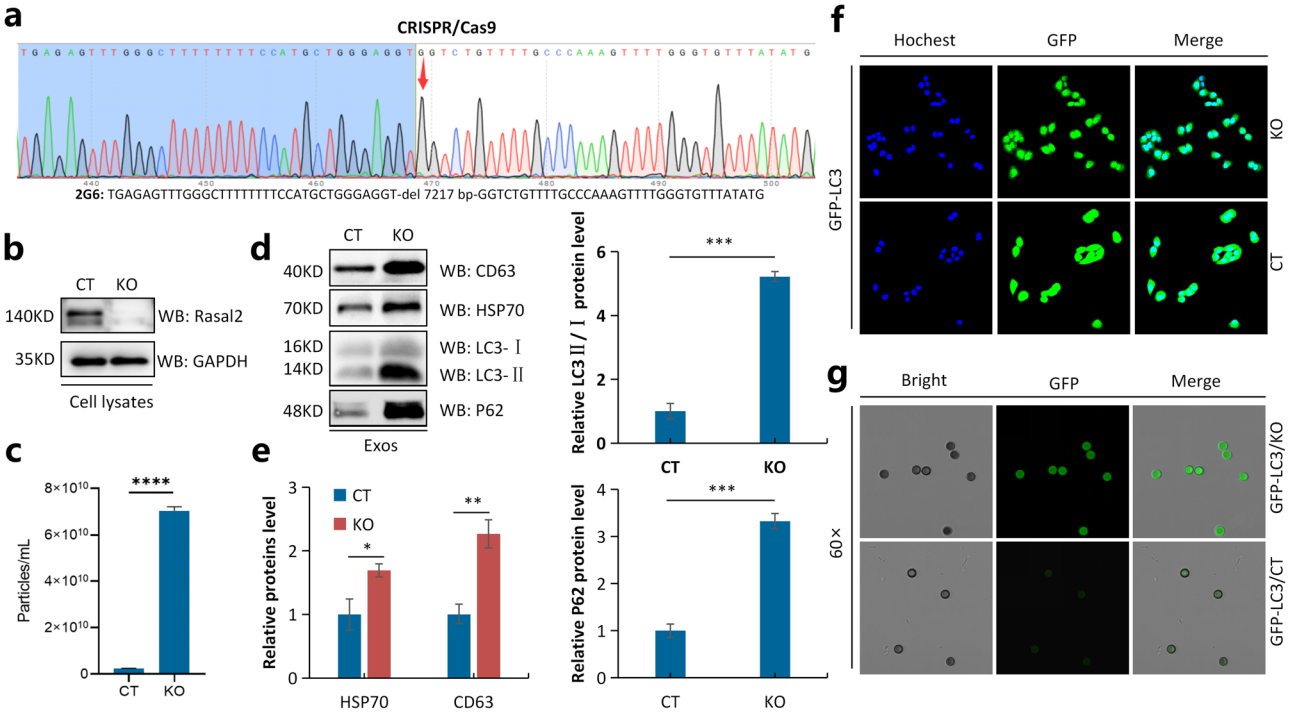

Fig. 2 Loss of Rasal2 promotes autophagic-exos secretion in TNBC. **a**, Construction of Rasal2 KO MDA-MB-231 cell lines by CRISPR/Cas9 technique. **b**, The protein expression of Rasal2 detected by western blot analysis. **c**, The effect of Rasal2 KO on exosomal secretion analyzed by NTA. **d-e**, Effects of Rasal2 KO on the expression levels of autophagic and exosomal marker proteins in exos. **f**, Establishment of CT and KO MDA-MB-231 cell lines with GFP-LC3 stable overexpression. **g**, Fluorescence intensity of magnetic beads-bound exos derived from CT and KO MDA-MB-231 cells stably overexpressing GFP-LC3

via quantitative analysis (Fig. 2d-e). To elucidate whether the accumulated autophagy-related proteins in exos were associated with autophagy, we applied GFP-LC3 plasmid to construct CT and KO MDA-MB-231 cell lines stably overexpressing LC3 and confirmed by fluorescence microscopy (Fig. 2f). Then Dynabeads® magnetic beads-bound exos isolated from the above constructed cells were photographed using confocal microscopy and the images presented a significant increase of green fluorescence intensity in beads-bound exos from KO MDA-MB-231 cells as compared with that in beads-bound exos from CT MDA-MB-231 cells (Fig. 2g), implying the loss of Rasal2 might affect autophagy process and the aggregation of autophagy-related proteins in exos induced by Rasal2 KO might probably derived from cell autophagy.

Loss of Rasal2 perturbs the autophagic pathway in TNBC

To validate the role of Rasal2 in cell autophagy, we observed the autophagosomes in CT and KO MDA-MB-231 cells by TEM and fluorescence microscope. The result of TEM displayed that more autophagosomes were generated in KO MDA-MB-231 cells than those in CT MDA-MB-231 cells (Fig. 3a). Meanwhile, the images under fluorescence microscope showed stronger fluorescence intensity in KO MDA-MB-231 cells with GFP-LC3 overexpression than that in GFP-LC3-overexpressed CT MDA-MB-231 cells (Fig. 3b-c). The above results indicated the absence of Rasal2 stimulated the production of autophagosomes. However, western blot analysis showed that the expression levels of autophagy marker proteins (LC3 and P62) were both obviously increased in KO MDA-MB-231 cells compared with those in CT MDA-MB-231 cells, which was further enhanced by bafilomycin A1 (BafA1), a late-stage autophagy inhibitor that blocks the fusion of autophagosomes with lysosomes (Fig. 3d), suggesting that aggregation of autophagy-associated proteins might be caused by the inhibition of autophagosomes degradation in lysosomes induced by Rasal2 KO.

To further investigate the effect of Rasal2 KO on the autophagic process, CT/KO MDA-MB-231 cell lines were transfected with the dual fluorescent plasmid mCherry-EGFP-LC3 and fluorescence microscopic detection manifested the proportion of autolysosomes (red puncta) in KO group was significantly decreased compared with that in CT group (43% vs. 88%), also further strengthened by BafA1 (20%), indicating that Rasal2 KO disrupted autophagic flux (Fig. 3e-f). However, the degradation of autophagosomes is closely related to the acidity of lysosomes, then lysosomal acidity was analyzed by fluorescence microscopy using Lyso-Tracker Green and the results exhibited that fluorescence intensity in KO group is significantly decreased compared to that in CT group (Fig. 3g-i). Taken together, these data

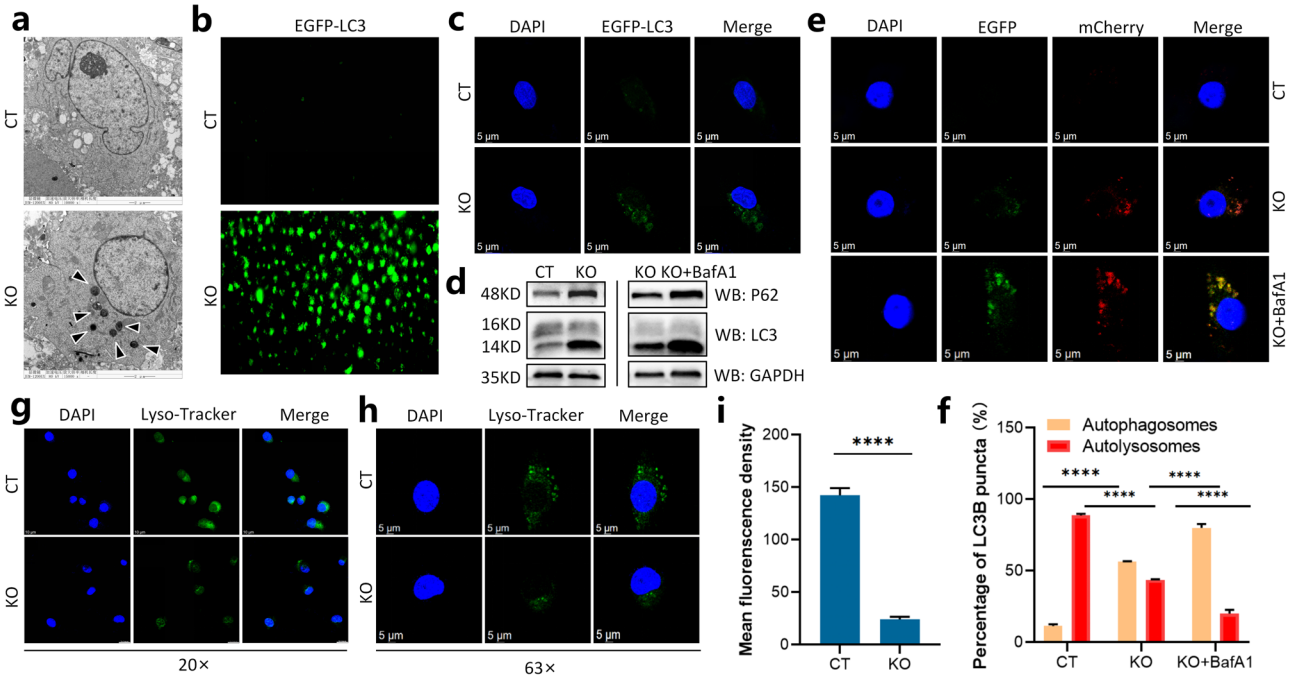

Fig. 3 Rasal2 KO disturbs the autophagic pathway. **a**, Observation of autophagosomes produced in CT/KO MDA-MB-231 cells by TEM. **b-c**, Analysis of fluorescent aggregation plot in CT/KO MDA-MB-231 cells with transient transfection of EGFP-LC3 plasmid. **d**, Detection of autophagy-related marker proteins expression in CT/KO MDA-MB-231 cells with or without BafA1 treatment by western blotting. **e-f**, Observation of autophagic flux in CT/KO MDA-MB-231 cells transfected with mCherry-EGFP-LC3 by confocal fluorescence microscopy and quantitative analysis of red and yellow fluorescence aggregation plots. **g-i**, The acidic probe Lyso-Tracker Green was used to detect lysosomal acidity in CT/KO MDA-MB-231 cells by confocal fluorescence microscope

demonstrated that the loss of Rasal2 prevents the degradation of autophagosomes in lysosomes by reducing lysosomal acidity.

Loss of Rasal2 induces secretory autophagy

To elucidate whether Rasal2 KO-induced the secretion of autophagic-exos is related to its regulation of autophagy, TEM was performed to observe the morphology, the size and the number of MVBs and ILVs in CT and KO MDA-MB-231 cells. We found that Rasal2 KO significantly expanded the size and increased the number of MVBs and ILVs, indicating the loss of Rasal2 promotes the generation of MVBs (Fig. 4a). Then confocal microscopy showed that the intensity of red fluorescent aggregation in KO MDA-MB-231 cells stained with CD63 antibody (CD63: specific transmembrane marker protein of MVBs) was stronger than that in CT MDA-MB-231 cells, which could be further intensified by BafA1 (Fig. 4b-c). Consistent with the above result, western blot analysis displayed the higher expression levels of CD63 and HSP70 in KO group than those in CT group, which could be also further facilitated by BafA1 (Fig. 4d-e). Additionally, we observed more colocalization of autophagosomes with MVBs in KO MDA-MB-231 cells transfected with EGFP-LC3 (green fluorescence) than that in EGFP-LC3-transfected CT MDA-MB-231 cells after these two kinds of cells were stained with CD63 antibody (red fluorescence), and this colocalization was further enhanced by BafA1 (Fig. 4f-g). Besides, a larger number of autophagosomes fused with MVBs was observed in KO group than that in CT group under TEM (Fig. 4h), demonstrating the accumulated autophagosomes induced by Rasal2 KO could fuse with MVBs when the lysosomal degradation pathway is blocked. In order to further prove that Rasal2 KO-induced the secretion of autophagic-exos is caused by its obstruction of autophagic pathway, we examined the effect of BafA1 on exos secretion in KO MDA-MB-231 cells. NTA results showed that KO MDA-MB-231 cells treated with BafA1 significantly increased the secretion of exos compared to KO group, while which could be significantly prevented by GW4869, an exosomal secretion inhibitor (Fig. 4i). Furthermore, western blot analysis revealed that the expression levels of autophagy-related proteins in exos derived from KO MDA-MB-231 cells co-incubated with BafA1 were significantly increased in comparison with those in exos derived from KO MDA-MB-231 cells (Fig. 4j). These results all suggest that the loss of Rasal2 induces secretory autophagy and the

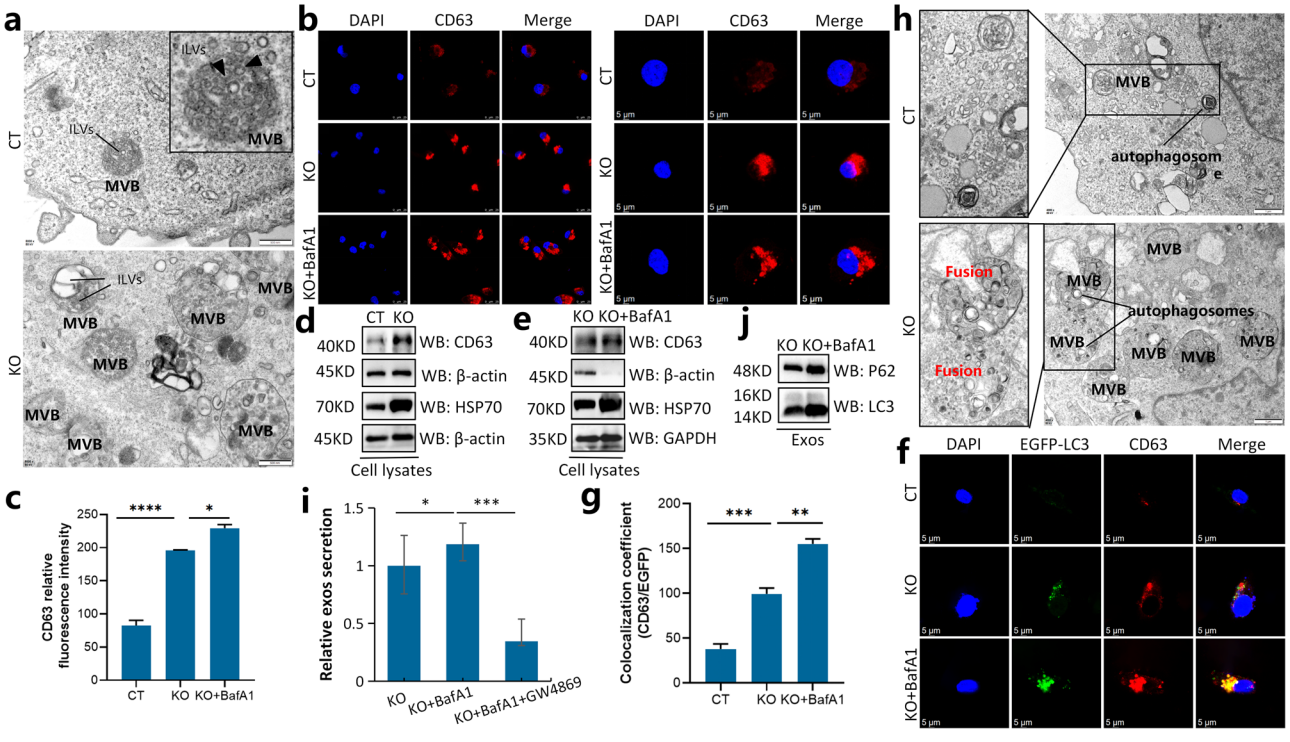

Fig. 4 Rasal2 KO induces secretory autophagy. **a**, The morphology, size and number of MVBs and ILVs in CT/KO MDA-MB-231 cells observed by TEM. **b-c**, The intensity of fluorescent aggregation plots in BafA1-treated CT/KO MDA-MB-231 cells stained with CD63 antibody observed by confocal microscopy. **d-e**, The expression levels of exosomal marker proteins in CT/KO MDA-MB-231 cells with BafA1 treatment. **f-g**, The colocalization of autophagosomes and MVBs in CT/KO MDA-MB-231 cells with BafA1 treatment observed by confocal microscopy. **h**, The fusion of autophagosomes with MVBs in CT/KO MDA-MB-231 cells observed by TEM. **i**, The amount of exos secretion from KO MDA-MB-231 cells with BafA1/GW4869 treatment detected by NTA. **j**, The expression of autophagy marker proteins in exos derived from KO MDA-MB-231 cells with BafA1 treatment detected by western blotting

undegraded autophagosomes aroused by Rasal2 KO-induced the obstruction of autophagy can be secreted extracellularly in the form of autophagic-exos.

Rab27a mediates Rasal2 KO-induced autophagic-exos secretion

To further explore the mechanism of autophagic-exos secretion induced by Rasal2 KO, we investigated the relationship between Rasal2 and Rab27a, an important protein that plays a cross role in the formation of autophagy and exos. Co-immunoprecipitation assay manifested the interaction between exogenous Rasal2 and Rab27a confrmed in HEK293T cells co-transfected with Myc-Rasal2 and Flag-Rab27a by using anti-Flag (M2) affinity purifcation (Fig. 5a). Meanwhile, the interaction between endogenous Rasal2 and Rab27a were also corroborative in MDA-MB-231 cells via anti-Rasal2 or anti-Rab27a affinity purification (Fig. 5b). Moreover, GTP-beads pull-down assay delineated that Rab27a-GTP level in Rasal2-KO MDA-MB-231 cells expressing Myc-Rasal2 was obviously decreased compared to that in Rasal2-null MDA-MB-231 cells, indicating Rasal2 inhibited the activity of Rab27a in MDA-MB-231 cells (Fig. 5c). To clarify the role of Rab27a in Rasal2 KO-induced autophagic-exos release, Rab27a knockdown (KD) in Rasal2-KO MDA-MB-231 (KO + KD) cells was generated by gene silencing technique using siRNA-mate plus transfection reagent and verified by western blot analysis (Fig. 5d). We found that the expression levels of autophagosomes marker proteins (LC3 and P62) and exos marker proteins (HSP70 and CD63) in exos derived from (KO + KD) cells were significantly lower than those in exos derived from KO cells (Fig. 5e). Besides, a significant reduction of exosomal secretion level was observed in (KO + KD) cells versus that in KO cells by using NTA (Fig. 5f), and a significant decrease of the red fluorescence intensity was detected in (KO + KD) cells stained with CD63 antibody than that in KO cells (Fig. 5i-j), while Rab27a overexpression (OE) in (KO + KD) cells significantly increased the expression of exosomal marker protein CD63 and promoted the secretion of exos (Fig. 5g-h). Also, the smaller size and the less number of MVBs and ILVs was found in (KO + KD) group than those in KO group by TEM observation (Fig. 5k-l). Additionally, confocal

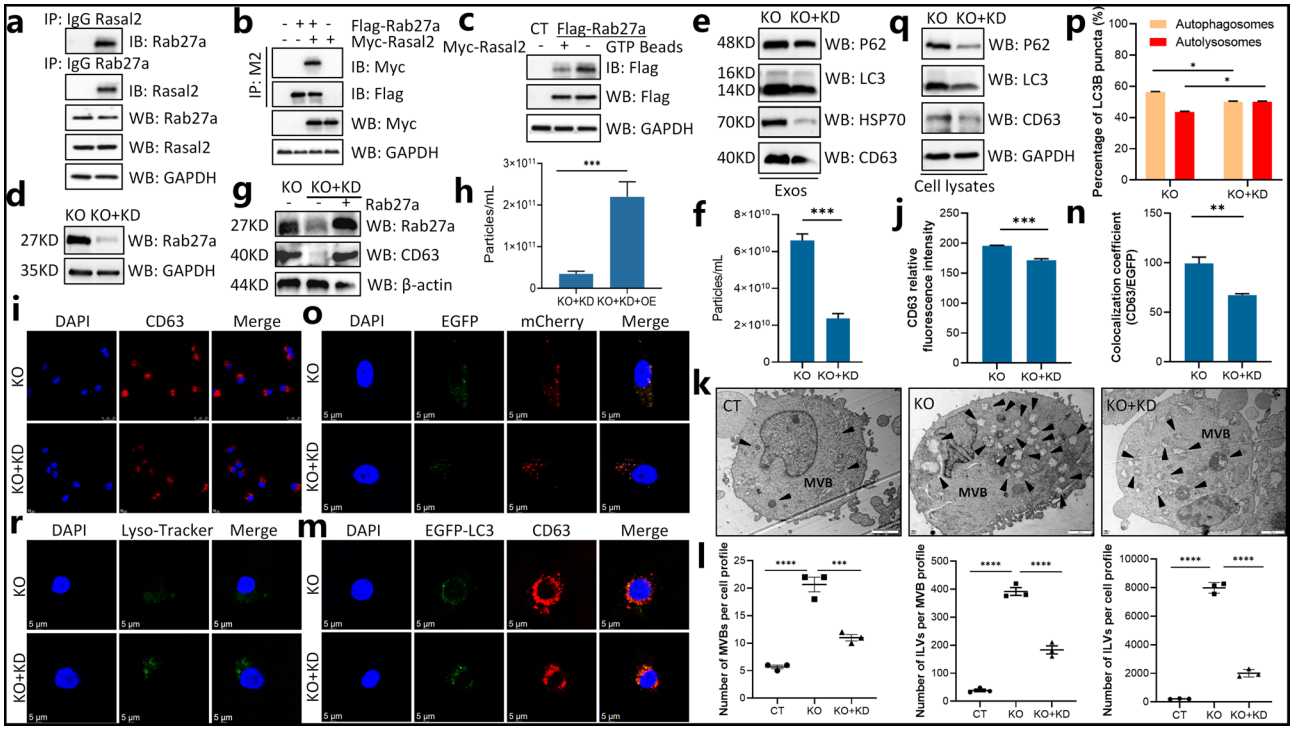

Fig. 5 Rab27a mediates Rasal2 KO-induced autophagic-exos secretion. **a**, The interaction between endogenous Rab27a and Rasal2 determined by immunoprecipitation assay. **b**, The interaction between exogenous Rab27a and Rasal2 determined by immunoprecipitation assay. **c**, The effect of Rasal2 on the activity of Rab27a detected by using GTP-beads pull-down assay. **d**, Establishment of Rab27a KD in Rasal2 KO cell lines. **e**, The effect of Rab27a KD on the expression of autophagy marker proteins and exosomal marker proteins in exos-derived from Rasal2-KO cells. **f**, The effect of Rab27a KD on exosomal secretion from Rasal2 KO cells detected by NTA. **g-h**, The effect of Rab27a overexpression on exosomal secretion from (KO + KD) cells. **i-j**, The effect of Rab27a KD on the fluorescence intensity of CD63 in Rasal2 KO cells. **k-l**, The effect of Rab27a KD on the size and number of MVBs and ILVs in Rasal2 KO cells. **m-n**, The effect of Rab27a KD on the colocalization of autophagosomes and MVBs in Rasal2 KO cells. **o-p**, The effect of Rab27a KD on autophagic flux in Rasal2 KO cells. **q**, The effect of Rab27a KD on the expression of autophagic and exosomal marker proteins in Rasal2 KO cells. **r**, The effect of Rab27a KD on lysosomal acidity of Rasal2 KO cells

microscopy observed less colocalization of MVBs with autophagosomes in (KO + KD) group than that in KO group (Fig. 5m-n). Importantly, the proportion of autolysosomes (red puncta) in (KO + KD) cells transfected with mCherry-EGFP-LC3 plasmid was significantly increased compared with that in KO group (50% vs. 43%) (Fig. 5o-p) and the degradation of autophagy-related proteins in (KO + KD) cells was also significantly increased in comparison with those in KO cells (Fig. 5q), indicating that Rasal2 KO-induced the obstruction of autophagic flux can be reversed by Rab27a KD. Furthermore, lysosomal acidity detected by fluorescence microscopy using LysoTracker Green was significantly increased in (KO + KD) group than that in KO group (Fig. 5r), Overall, these findings corroborated Rab27a mediates Rasal2 KO-induced secretory autophagy and autophagic-exos secretion.

Inhibition of secretory autophagy promotes TNBC progression

To clarify the role of Rab27a-mediated Rasal2 KO-induced secretory autophagy in TNBC cell progression, we firstly examined the expression levels of Rasal2 in different TNBC cells and the result showed Rasal2 expression levels in TNBC cells were significantly increased compared with that in MCF10A normal breast cells (Fig. 6a-b). CCK-8 assay and clony formation assay displayed that Rasal2 KO significantly inhibited cell proliferation and clony formation (Fig. 6c-e). Transwell migration and invasion assays elucidated that Rasal2 KO significantly inhibited TNBC cell migration and invasion compared to those in CT group through microscopy observation and quantitative analysis (Fig. 6f-g). Consistently, scratch wound assay also showed that Rasal2 KO have a significant inhibitory effect on cell migration (Fig. 6h-i). However, the inhibition of cell proliferation, migration and invasion induced by Rasal2 KO in all the above results could be reversed by Rab27a KD. Collectively, these data validated that Rab27a KD promotes TNBC progression by attenuating Rasal2 KO-induced secretory autophagy.

Inhibition of secretory autophagy promotes xenograft tumor growth in mice

To further verify whether Rab27a plays a role in Rasal2-regulated the growth of xenograft tumor in mice, tumor xenograft animal models for MDA-MB-231 cells (CT, KO, KO + KD) were established in BALB/c nude mice (Fig. 7a). In accord with the results in vitro, the growth curve of xenograft tumor showed that Rasal2 KO significantly decreased the rate of tumor growth in vivo, while Rab27a KD in KO cells significantly reversed the inhibitory effect of Rasal2 KO-induced on tumor growth, with

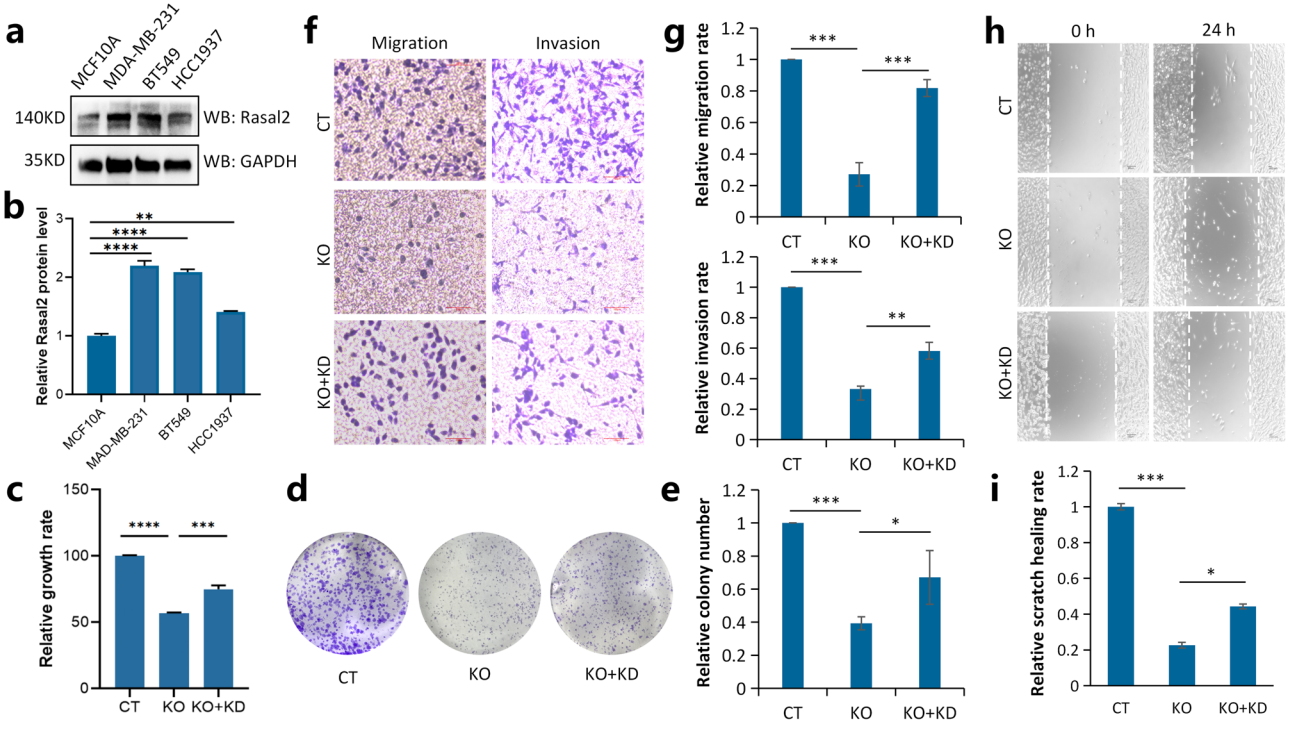

Fig. 6 Inhibition of secretory autophagy promotes TNBC progression in vitro. **a-b**, The protein expression of Rasal2 in TNBC cells and normal breast cells. **c-e**, The effect of Rab27a on TNBC cell proliferation and clony formation regulated by Rasal2 evaluated by CCK-8 assay and clony formation assay. **f-g**, The effect of Rab27a on Rasal2-regulated TNBC cell migration and invasion measured by transwell assays. **h-i**, The effect of Rab27a on Rasal2-regulated TNBC cell migration analyzed by the wound healing assay

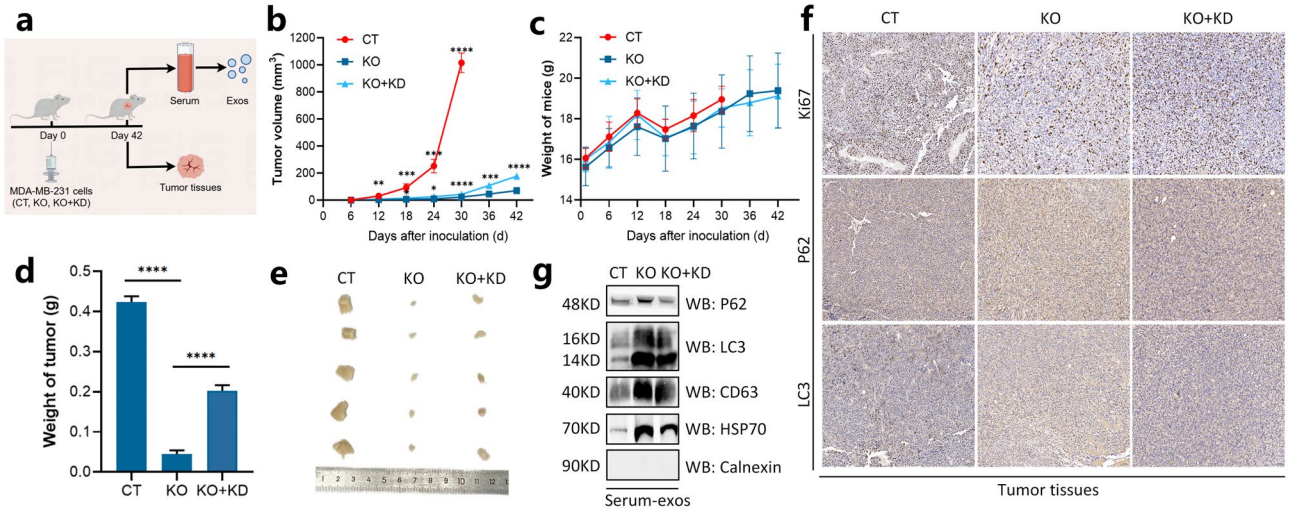

Fig. 7 Inhibition of secretory autophagy promotes xenograft tumor growth in mice. **a**, xenograft animal models for MDA-MB-231 cells (CT, KO, KO + KD) were established in BALB/c nude mice. **b**, The growth curves of the tumor in mice after inoculating with MDA-MB-231 cells (CT/KO/KO + KD). **c**, The changes curve of mice weight after inoculating with MDA-MB-231 cells (CT/KO/KO + KD). **d**, Average tumor weight in CT/KO/KO + KD group. **e**, Photographs of tumors in CT/KO/KO + KD group. **f**, Immunohistochemistry analysis of proliferation-related and autophagy-related proteins. **g**, Expression of autophagic and exosomal marker proteins in exos derived from the serum of mice in CT/KO/KO + KD group

no significant difference in weight change of all mice (Fig. 7b-c). In addition, the result of average tumor weight was shown in Fig. 7d, and the photographs of the tumors in each group were shown in Fig. 7e. Moreover, immunohistochemistry analysis showed the lower expression level of proliferation-associated protein Ki67 and the higher expression levels of autophagy-related proteins (P62 and LC3) in tumor tissues of KO group than those in tumor tissues of CT group, while the expression levels of the above proteins were all reversed after Rab27a KD in KO group (Fig. 7f). Also, exos derived from the serum of xenograft tumor mice in KO group expressed more autophagy-associated proteins (P62 and LC3) and exos marker proteins (HSP70 and CD63) compared with those in serum-derived exos from mice in CT group. Similarly, the expression levels of the above proteins all can be reversed after Rab27a KD in KO group (Fig. 7g). Taken together, these data suggest that the regulation of Rasal2 KO-induced secretory autophagy by Rab27a is associated with TNBC progression.

Discussion

Rasal2 exerts either pro- or anti-oncogenic behavior in different human cancers and it has been considered to be depend on the tumor type or cell context [10, 39]. In our previous study, we have demonstrated that the functions of Rasal2 acting as a promoter or suppressor in breast cancers are determined by the phosphorylation level of Rasal2 and the effects of phosphorylated Rasal2 on breast cancers are exos-mediated [14]. Here, an in-depth investigation was conducted to further explore the specific mechanisms of the regulatory function of Rasal2 in exos secretion.

In the present study, we successfully constructed Rasal2-KO MDA-MB-231 cell lines and isolated the exos from the above cells. Then, the exos were characterized by their morphology, particle size distribution, potential as well as exosomal marker proteins, all of them met the requirements of the International Society for Extracellular Vesicles (ISEV) for exos identification. Subsequently, we quantitatively analyzed the secretion of exos derived from Rasal2-KO cells and found that the loss of Rasal2 obviously stimulates the exos secretion. Furthermore, the secreted exos aggregated abundant autophagy marker proteins, validated via the proteins expression levels performed by western blot analysis and the fluorescence intensity in immunomagnetic beads-enriched exos purified from Rasal2-KO cells stably overexpressing GFP-LC3 observed by confocal microscopy. LC3, also called MAP1LC3 (microtubule associated protein 1 light chain 3), involved in the autophagosomal biogenesis, is the most reliable and recognized marker of autophagosomes [40, 41], suggesting that Rasal2 KO might promote autophagic-exos secretion in TNBC.

To verify whether the accumulation of autophagy marker proteins in the exos is originated from autophagy, we explored the regulation of autophagic pathway by Rasal2 and corroborated that Rasal2 KO promoted the production of autophagosomes but prevented the degradation of autophagosomes in lysosomes by TEM, confocal microscopy and western blot analysis, further validated by the the blockage of autophagic flux induced by Rasal2 KO via using the mCherry-EGFP-LC3 reporter.

The regulatory effects above of Rasal2 KO on autophagy can be enhanced by BafA1, a typical lysosomal inhibitor which could decrease lysosomal acidity to impair lysosomal degradative function [42, 43], Moreover, it was affirmed that the disturbance of the autophagic pathway is attributed to the decrease of H + concentration in lysosomes by using the fluorescent probe Lyso-Tracker Green to indicate the changes of PH in Rasal2 KO cells.

To further determine whether the accumulation of autophagy proteins in secreted exos is derived from the undegraded autophagosomes produced by Rasal2 KO, we observed the morphology, size and number of MVBs and ILVs in MVBs by TEM and detected the expression of CD63 (a exosomal marker protein that exists on the membrane of MVBs in cells) by immunofluorescence analysis and western blot analysis, confirming that Rasal2 KO dramatically increases the size and the number of MVBs and ILVs, which can be further promoted by BafA1. Subsequently, we examined the colocalization of MVBs and autophagosomes in Rasal2-KO cells by confocal microscopy and TEM, respectively, and affirmed that Rasal2 KO-induced the accumulated autophagosomes fused with MVBs. Furthermore, the fusion of autophagosomes with MVBs could also be promoted by BafA1. In addition, we detected the amount of exos secretion and the expression levels of autophagy-related proteins in secreted exos by BafA1 and GW4869, an exosomal secretion inhibitor, all the findings demonstrated that Rasal2 KO stimulates autophagic-exos secretion and induces secretory autophagy. Secretory autophagy, first proposed by Ponpuak et al. [44]., means that autophagosomes formed in the process of autophagy are not only transported to lysosomes for degradation, but also fused with MVBs to eventually form exos (i.e., autophagic-exos) when lysosomal dysfunction or the blockage of autophagosomes degradation [25, 26].

Accumulating studies have proved that the process of autophagy formation and vesicle transport intersects in many places. Rab family, which play a molecular "switch" role in membrane transport and also participate in autophagy process [35, 45]. Rab27a, responsible for the docking and fusion of MVBs with the plasma membrane, is required for exos formation and secretion [46]. We confirmed that Rasal2 interacts with Rab27a and inhibits the activity of Rab27a by co-immunoprecipitation analysis. To further clarify the role of Rab27a in Rasal2 KO-induced the secretion of autophagic-exos, Rab27a KD in Rasal2 KO (KO + KD) MDA-MB-231 cell lines were established, and we found that Rab27a KD significantly reduced the secretion of exos, while the level of exosomal secretion was significantly increased by reintroducing Rab27a in (KO + KD) cells. Furthermore, Rab27a KD significantly decreased the content of autophagy-related proteins in the secreted exos induced by Rasal2 KO, significantly decreased the size and number of MVBs and the fusion of MVB with autophagosomes, while significantly promoted autophagic flux by increasing the acidity of lysosomes, demonstrating Rab27a mediates Rasal2 KO-induced autophagic-exos secretion.

Next, we examined the effect of Rasal2 KO-induced secretory autophagy on TNBC cell progression in vitro and in vivo. We demonstrated that Rasal2 was highly expressed in various types of TNBC cells, while Rasal2 KO inhibited cell proliferation verified by CCK-8 assay and clony formation assay, and cell migration and invasion were also inhibited by Rasal2 KO confirmed via scratch healing assay and transwell assay, while all of which could be reversed by Rab27a KD in Rasal2 KO cells. Additionally, the rate of tumor growth and tumor weight of xenografted mice inoculated with Rasal2 KO cells were significantly reduced compared with those in CT group, and immunohistochemical analysis showed that the expression of proliferation-related protein Ki67 (as a prognostic and predictive marker [47, 48]) in xenograft tumor tissues of KO group was significantly decreased. Western blot analysis showed that the expression levels of the autophagy-related proteins (LC3 and P62) and exos marker proteins (CD63 and HSP70) in serum-derived exos of mice were significantly increased, consistent with the results of immunohistochemical analysis. However, all the effects above induced by Rasal2 KO could be reversed by Rab27a KD in Rasal2 KO cells. In conclusion, these findings demonstrated that Rab27a inhibits TNBC progression by promoting the secretion of autophagic-exos induced by the loss of Rasal2. This study not only expands the understanding of the regulatory effect of Rasal2 on exosomal secretion and provides new insights into the role of Rab27a in tumor progression, but also reveals the coordinated mechanisim of lysosomal homeostasis and exosomal secretion in cancer development from the perspective of tumor microenvironment, which might provide a potential therapeutic strategy for TNBC, and plasma-derived autophagic-exos might act as non-invasive biomarkers to dynamically monitor lysosome function in TNBC therapy.

Conclusions

Collectively, we elucidated the regulation of Rasal2 on autophagy and autophagic-exos secretion, and confirmed the important role of Rab27a in Rasal2-regulated the secretion of autophagic-exos through in vivo and in vitro experiments, indicating the coordination mechanism of autophagy-exos signaling pathway in TNBC progression and providing a theoretical basis for the diagnosis and treatment of TNBC.

Abbreviations

TNBC	Triple-negative breast cancer
Rasal2	Ras protein activator like 2

EVs	Extracellular vesicles
Exosomes	Exos
MVBs	Multivesicular bodies
ILVs	Intraluminal vesicles
SQSTM1/P62	Sequestosome 1
MAP1LC3/LC3	Microtubule-associated protein 1 light chain 3
LAMP3/CD63	Lysosomal-associated membrane protein-3
HSP70	Heat shock protein 70
Rab27a	Ras-related protein rab-27a
BafA1	Bafilomycin A1
TEM	Transmission electron microscopy
NTA	Nanoparticle tracking analysis
ER	Estrogen receptor
PR	Progesterone receptor
HER2	Human epidermal growth factor receptor 2
EMT	Epithelial-mesenchymal transformation

Acknowledgements
Not applicable.

Author contributions
Study design: W.X.; Experimental operation: W.X. and Q.GC. Data acquisition: Q.GC. and M.LL.; Data analysis: M.LL., K.YS. and T.XJ.; Research writing and revision of the manuscript: W.X. and Y.KN.; Study supervision: H.YT.

Funding
This work was supported by grants from the National Natural Science Foundation of China (Grant No. 82404689) and Natural Science Foundation of Shandong Province (Grant No. ZR2022QH210).

Data availability
The datasets used or analyzed during the study are available from the corresponding author on reasonable request.

Declarations

Ethics approval and consent to participate
Animal experiments were approved by the Animal Ethical Committee of Qingdao University.

Consent for publication
All authors agree to publish.

Competing interests
The authors declare no competing interests.

Author details
[1]Department of Pharmacology, School of Basic Medicine, Qingdao University, 308 Ningxia Road, Qingdao 266071, China
[2]Department of Respiratory Medicine, Weifang Second People's Hospital, Weifang, China

Received: 27 February 2025 / Accepted: 23 April 2025
Published online: 14 May 2025

References

1. Sung H, Ferlay J, Siegel RL, et al. Global Cancer statistics 2020: GLOBOCAN estimates of incidence and mortality worldwide for 36 cancers in 185 Countries[J]. CA Cancer J Clin. 2021;71(3):209–49.
2. Chiang YF, Huang KC, Chen HY et al. Hinokitiol inhibits breast Cancer cells in vitro Stemness-Progression and Self-Renewal with apoptosis and autophagy modulation via the CD44/Nanog/SOX2/Oct4 Pathway[J]. Int J Mol Sci. 2024;25(7).
3. Liedtke C, Mazouni C, Hess KR, et al. Response to neoadjuvant therapy and Long-Term survival in patients with Triple-Negative breast Cancer[J]. J Clin Oncol. 2023;41(10):1809–15.
4. Mehraj U, Mushtaq U, Mir MA, et al. Chemokines in triple-negative breast cancer heterogeneity: new challenges for clinical implications[J]. Semin Cancer Biol. 2022;86(Pt 2):769–83.
5. Hamdy NM, Basalious EB, El-Sisi MG, et al. Advancements in current one-size-fits-all therapies compared to future treatment innovations for better improved chemotherapeutic outcomes: a step-toward personalized medicine[J]. Curr Med Res Opin. 2024;40(11):1943–61.
6. Hamdy NM, El-Sisi MG, Ibrahim SM, et al. In Silico analysis and comprehensive review of circular-RNA regulatory roles in breast diseases; a step-toward non-coding RNA precision[J]. Pathol Res Pract. 2024;263:155651.
7. Cao L, Zhu S, Lu H, et al. Helicobacter pylori-induced RASAL2 through activation of nuclear Factor-κB promotes gastric tumorigenesis via β-catenin signaling Axis[J]. Gastroenterology. 2022;162(6):1716–31.
8. McLaughlin SK, Olsen SN, Dake B, et al. The RasGAP gene, RASAL2, is a tumor and metastasis suppressor[J]. Cancer Cell. 2013;24(3):365–78.
9. Pan Y, Tong J, Lung R, et al. RASAL2 promotes tumor progression through LATS2/YAP1 axis of Hippo signaling pathway in colorectal cancer[J]. Mol Cancer. 2018;17(1):102.
10. Olsen SN, Wronski A, Castaño Z, et al. Loss of RasGAP tumor suppressors underlies the aggressive nature of luminal B breast Cancers[J]. Cancer Discov. 2017;7(2):202–17.
11. Koh SB, Ross K, Isakoff SJ, et al. RASAL2 confers collateral MEK/EGFR dependency in chemoresistant Triple-Negative breast Cancer[J]. Clin Cancer Res. 2021;27(17):4883–97.
12. Feng M, Bao Y, Li Z, et al. RASAL2 activates RAC1 to promote triple-negative breast cancer progression[J]. J Clin Invest. 2014;124(12):5291–304.
13. Fang JF, Zhao HP, Wang ZF, et al. Upregulation of RASAL2 promotes proliferation and metastasis, and is targeted by miR-203 in hepatocellular carcinoma[J]. Mol Med Rep. 2017;15(5):2720–6.
14. Wang X, Qian C, Yang Y, et al. Phosphorylated Rasal2 facilitates breast cancer progression[J]. EBioMedicine. 2019;50:144–55.
15. Wang X, Yin X, Yang Y. Rasal2 suppresses breast cancer cell proliferation modulated by secretory autophagy[J]. Mol Cell Biochem. 2019;462(1–2):115–22.
16. Perrin P, Janssen L, Janssen H, et al. Retrofusion of intralumenal MVB membranes parallels viral infection and coexists with exosome release[J]. Curr Biol. 2021;31(17):3884–93.
17. Wang X, Liu Y, Qin H et al. RIP1 mediates Manzamine-A-Induced secretory autophagy in breast Cancer[J]. Mar Drugs. 2023;21(3).
18. Hamdy NM, Zaki MB, Rizk NI, et al. Unraveling the NcRNA landscape that governs colorectal cancer: A roadmap to personalized therapeutics[J]. Life Sci. 2024;354:122946.
19. Lucien F, Gustafson D, Lenassi M, et al. MIBlood-EV: minimal information to enhance the quality and reproducibility of blood extracellular vesicle research[J]. J Extracell Vesicles. 2023;12(12):e12385.
20. Cano A, Ettcheto M, Bernuz M, et al. Extracellular vesicles, the emerging mirrors of brain physiopathology[J]. Int J Biol Sci. 2023;19(3):721–43.
21. Kalluri R, LeBleu VS. The biology, function, and biomedical applications of exosomes[J]. Science. 2020;367(6478).
22. Pegtel DM, Gould SJ. Exosomes[J]. Annu Rev Biochem. 2019;88:487–514.
23. Ohsumi Y. Historical landmarks of autophagy research[J]. Cell Res. 2014;24(1):9–23.
24. Klionsky DJ, Petroni G, Amaravadi RK, et al. Autophagy in major human diseases[J]. EMBO J. 2021;40(19):e108863.
25. Debnath J, Leidal AM. Secretory autophagy during lysosome Inhibition (SALI)[J]. Autophagy. 2022;18(10):2498–9.
26. Solvik TA, Nguyen TA, Tony LY et al. Secretory autophagy maintains proteostasis upon lysosome inhibition[J]. J Cell Biol. 2022;221(6).
27. Debnath J, Gammoh N, Ryan KM. Autophagy and autophagy-related pathways in cancer[J]. Nat Rev Mol Cell Biol. 2023;24(8):560–75.
28. Amaravadi RK, Kimmelman AC, Debnath J. Targeting autophagy in cancer: recent advances and future Directions[J]. Cancer Discov. 2019;9(9):1167–81.
29. Cunha LD, Yang M, Carter R, et al. LC3-Associated phagocytosis in myeloid cells promotes tumor immune Tolerance[J]. Cell. 2018;175(2):429–41.
30. Homma Y, Hiragi S, Fukuda M. Rab family of small GTPases: an updated view on their regulation and functions[J]. FEBS J. 2021;288(1):36–55.
31. Xiao GY, Tan X, Rodriguez BL, et al. EMT activates exocytotic Rabs to coordinate invasion and immunosuppression in lung cancer[J]. Proc Natl Acad Sci U S A. 2023;120(28):e2074691176.
32. Pfeffer SR. Two Rabs for exosome release[J]. Nat Cell Biol. 2010;12(1):3–4.
33. Song L, Tang S, Han X, et al. KIBRA controls exosome secretion via inhibiting the proteasomal degradation of Rab27a[J]. Nat Commun. 2019;10(1):1639.
34. Gutierrez MG, Munafó DB, Berón W, et al. Rab7 is required for the normal progression of the autophagic pathway in mammalian cells[J]. J Cell Sci. 2004;117(Pt 13):2687–97.

35. Zhao YG, Codogno P, Zhang H. Machinery, regulation and pathophysiological implications of autophagosome maturation[J]. Nat Rev Mol Cell Biol. 2021;22(11):733–50.
36. Théry C, Amigorena S, Raposo G et al. Isolation and characterization of exosomes from cell culture supernatants and biological fluids[J]. Curr Protoc Cell Biol. 2006; Chap. 3:3–22.
37. Lee YJ, Shin KJ, Jang HJ, et al. GPR143 controls ESCRT-dependent exosome biogenesis and promotes cancer metastasis[J]. Dev Cell. 2023;58(4):320–34.
38. Wang X, Yin X. Panobinostat inhibits breast cancer progression via Vps34-mediated Exosomal pathway[J]. Hum Cell. 2023;36(1):366–76.
39. Shen J, Wang Y, Hung MC. RASAL2: wrestling in the combat of Ras activation[J]. Cancer Cell. 2013;24(3):277–9.
40. Mareninova OA, Jia W, Gretler SR, et al. Transgenic expression of GFP-LC3 perturbs autophagy in exocrine pancreas and acute pancreatitis responses in mice[J]. Autophagy. 2020;16(11):2084–97.
41. De Mazière A, van der Beek J, van Dijk S, et al. An optimized protocol for immuno-electron microscopy of endogenous LC3[J]. Autophagy. 2022;18(12):3004–22.
42. Mauthe M, Orhon I, Rocchi C, et al. Chloroquine inhibits autophagic flux by decreasing autophagosome-lysosome fusion[J]. Autophagy. 2018;14(8):1435–55.
43. Brun S, Bestion E, Raymond E, et al. GNS561, a clinical-stage PPT1 inhibitor, is efficient against hepatocellular carcinoma via modulation of lysosomal functions[J]. Autophagy. 2022;18(3):678–94.
44. Ponpuak M, Mandell MA, Kimura T, et al. Secretory autophagy[J]. Curr Opin Cell Biol. 2015;35:106–16.
45. Tremel S, Ohashi Y, Morado DR, et al. Structural basis for VPS34 kinase activation by Rab1 and Rab5 on membranes[J]. Nat Commun. 2021;12(1):1564.
46. Bobrie A, Krumeich S, Reyal F, et al. Rab27a supports exosome-dependent and -independent mechanisms that modify the tumor microenvironment and can promote tumor progression[J]. Cancer Res. 2012;72(19):4920–30.
47. Yerushalmi R, Woods R, Ravdin PM, et al. Ki67 in breast cancer: prognostic and predictive potential[J]. Lancet Oncol. 2010;11(2):174–83.
48. Sohail A, Hacker J, Ryan T, et al. Nasal polyp antibody-secreting cells display proliferation signature in aspirin-exacerbated respiratory disease[J]. J Allergy Clin Immunol. 2024;153(2):527–32.

Publisher's note